A New Parsimonious Methodology of Mapping the Spatial Variability of Annual Maximum Rainfall in Mountainous Environments

G. BONI
CIMA Research Foundation, Savona, and DIST, University of Genova, Genova, Italy

A. PARODI
CIMA Research Foundation, Savona, Italy

F. SICCARDI
CIMA Research Foundation, Savona, and DIST, University of Genova, Genova, Italy

(Manuscript received 2 March 2007, in final form 6 December 2007)

ABSTRACT

The estimation of rare frequency rainfall is an essential prerequisite for the design of engineering structures and to determine risk areas. Index-based methods are among the most applied for regional frequency analysis of hydrological variables such as discharge and rainfall and comprise two stages: the mapping of a scale or "index" factor and the derivation of rainfall growth curves. The underlying hypothesis of these methods is that cumulative distribution functions of a certain random variable can be assumed homogeneous on a given region, except for the index factor, which varies spatially in that region and is often represented by the expected value of the random variable itself at a given location. Methods either to single out homogeneous regions or to evaluate the index factor can be purely statistical and physically based.

In this paper a robust and transferable physically based methodology is proposed to estimate the index factor for rainfall in mountainous regions referred to in the following text as "index rainfall." Index rainfall is defined as the expected value of annual rainfall maxima recorded in a fixed time window: a time window of 1 h is used. Reliable estimates of the index rainfall are obtained at ungauged sites by applying a relationship, based on a multivariate linear regression obtained at gauged sites, of rainfall and selected synthetic descriptors for atmospheric climate and orography. An extended and general set of descriptors is chosen from parameters that are considered in the literature to affect rainfall intensity. The relevant relief descriptors, defining slope, elevation, orientation, etc., at a given location, are extracted from digital elevation models (DEMs). A 2D Fourier series analysis of the DEM is performed and a spectral analysis is carried out to single out the components with the highest morphological information content. The synthetic relief descriptors are evaluated along different cross sections of the 2D truncated Fourier series to single out the role of the prevailing convection direction of extreme rainfall-producing meteorological patterns. The optimal descriptor subset for the study area is then extracted to maximize transferability of the method. Application to the Italian and French Alps and the Apennines shows encouraging results. Descriptor subset extraction has been tested and validated on independent subsets of index rainfall estimates in the regions. Results demonstrate that the proposed method is robust, transferable, and reliable for the evaluation of the index rainfall in ungauged sites.

1. Introduction

A frequency analysis on hydrometeorological variables, such as rainfall or river discharge, has a number of applications in the field of environmental and civil engineering and hydrometeorology, ranging from risk assessment (Kuligowski and Barros 1998; Bocchiola et al. 2003; Siccardi et al. 2005) and hydraulic structure design (Chow et al. 1988) to the improvement of the understanding of extreme rainfall hydrometeorology (Boni et al. 2006). In a frequency analysis, regional procedures are the most robust, since they minimize the estimation error due to sample size. Among them, index-based methods are the most used (Bobee and Rasmussen 1995). The main assumption underlying index-based methods is that hydrological variables at different sites within a "homogeneous" region follow the

Corresponding author address: A. Parodi, CIMA Research Foundation, Via Magliotto 2, 17100 Savona, Italy.
E-mail: antonio@cima.unige.it

DOI: 10.1175/2007JHM900.1

same probability distribution except in a scale or "index" factor. The latter is represented by the expected value of the variable itself at a given location. Methods to contour homogeneous regions have a long history and are quite well established and several good examples can be found in literature (Cavadias 1990; Nathan and McMahon 1990; Cunnane 1987; Fiorentino et al. 1987; Gabriele and Arnell 1991; Bobee and Rasmussen 1995).

Despite its relevance in risk assessment and hydraulic structure design, as testified by some recent studies (Dalrymple 1960; Reed 1994; Faulkner and Prudhomme 1998; Stewart et al. 1999; Weisse and Bois 2001; Renard and Langa 2007), less attention has been paid to the problem of index factor evaluation, often solved through purely statistical methods adapted to each test case.

The influence of topography on precipitation can be attributed primarily to localized disturbances of the vertical structure of the atmosphere. Moreover, the airflow over a topographic barrier leads to the ascent of water-rich, relatively warm air from low elevations. The forced ascent of moist air triggers condensation, the formation and growth of clouds, and ultimately, precipitation events at high elevations, especially along the windward slopes of topographic barriers (Barros and Lettenmaier 1993, 1994). Therefore, in this study we want to provide a general and robust methodology for a rainfall index factor estimation in mountainous regions.

Mountains are characterized, from the hydrological point of view, by small steep river catchments that, after intense and short-duration rainfall events (Kuligowski and Barros 1998; Ferraris et al. 2002; Siccardi et al. 2005), can generate flash floods in just a few hours. Therefore, for practical applications, rainfall frequency analysis focuses on annual rainfall maxima recorded in short time windows (e.g., one or few hours).

Following Rosso and Burlando (1996), we introduce the definition of annual rainfall maxima in a rigorous mathematical framework. Let us consider $R(\mathbf{x}, t)$ the random variable describing the continuous process of the rainfall rate at time t measured at a point in space $\mathbf{x}$ at a gauged site. The accumulated rainfall recorded over a given time interval d can be defined as

$$R_d(\mathbf{x}, t) = \int_{t-\frac{d}{2}}^{t+\frac{d}{2}} R(\mathbf{x}, \zeta)\, d\zeta. \tag{1}$$

The maximum value of $R_d(\mathbf{x}, t)$ in a time period of one year, that is, the annual rainfall maxima recorded in time window τ, is

$$H_d(\mathbf{x}, t) = \max[R_d(\mathbf{x}, t): t_0 < t < t_0 + \tau], \tag{2}$$

where $\tau = 1$ yr. Here, the index parameter, or "index rainfall," is defined as $\mathrm{IR}_d = E(H_d)$ and its spatial pattern is what we want to estimate.

In literature, efforts have been made in mapping average daily, monthly, or seasonal accumulated rainfall depths in areas with complex orography. These mapping methods vary from simple geostatistical methods, like the inverse distance technique (Tabios and Salas 1985) and kriging (Journel and Huijbregts 1978), to more complex techniques that, ever since the pioneering work of Spreen (1947), have investigated the relationships between precipitation and landscape properties (i.e., altitude, slope, distance from the coastline, and exposure).

Such mapping methods can be classified into two main categories: 1) purely morphological and 2) based on meteorological and morphological ingredients. Examples of the former, which relates rainfall variability in space only to terrain morphology, are provided by Basist and Bell (1994) who studied statistical relationships between approximately 10 topographic variables and the spatial distribution of mean annual precipitation over distinct mountainous regions around the world, while Wotling et al. (2001) provided a method to interpolate hourly rainfall accumulations for a given threshold [peak overthreshold sampling (POT)] on the volcanic island of Tahiti. Their method uses a regression algorithm based on the principal component analysis of a digital elevation model able to supply a limited set of synthetic variables describing the topographical environment. Methods relying on meteorological and morphological considerations introduce a dependency of rainfall climatology spatial patterns on meteorological factors. Daly et al. (1994) presented a climate analysis system, named the Parameter-elevation Regressions on Independent Slopes Model (PRISM), which uses point data, a digital elevation model (DEM), and other spatial datasets to generate gridded estimates of monthly and annual rainfall amounts over the western United States by using a combination of climatological and statistical parameters for the analysis of orographic precipitation. Johansson and Chen (2003) studied the influence of wind and topography on daily precipitation distribution in Sweden and proposed a statistical model, accounting for topographic influence, by using approximately 20 regression variables (morphological and meteorological), to describe basic patterns of precipitation distribution.

All the described methods focus on variables and aims, which differ from those of regional rainfall frequency analysis in mountainous regions. They are very efficient at describing spatial patterns of average rainfall accumulated during long time windows (i.e., day,

month, season), since the main goal is the description of rainfall climatology in the study region. Moreover, they are designed for the specific test case and thus, they cannot be easily applied to other locations. However, they represent an excellent starting point for the analysis presented here.

In the regional frequency analysis of H_d, the need of IR_d maps for ungauged sites, requires, especially in mountainous areas where the station density is low, the investigation of the relationships in precipitation, extreme meteorological events, climatology, and topography. The aim of this study is to develop a general and robust mapping method for IR_d over mountainous areas by using a general descriptor set extracted from easily accessible information about topography and intense rainfall climatology. A first general set of descriptors is chosen from climate parameters, which are considered in the literature to affect rainfall intensity in complex orography areas. This choice is supported by examining in detail the scales of the different terms involved in the advection-convection model of Smith and Barstad (2004). Since extreme rainfall is of concern, we focus on descriptors related to high-intensity orographic rainfall and in particular to the sample mean of annual rainfall maxima H_d defined by (2).

In section 2, we describe the criteria used for the selection of this first set. The innovation of the method is that this first set of descriptors, general in their nature for orographic precipitation, is sampled through an objective procedure, based on the regression between IR_d and each descriptor. The form of the regression function and the elements of the subset are defined on the basis of the observed IR_d, estimated by the sample mean of local H_d at a rain gauge site. This allows us to obtain an optimal descriptor subset for the study area. This procedure maximizes the transferability of the method and provides suggestions about the physics of the orographic rainfall in the study area, by speculating on the relations between the general set and the optimized one. Section 2 also describes how to obtain a general form for the regression function focusing on the duration $d = 1$ h. Section 3 presents the method proposed for the extraction of the relevant relief descriptors, defining slope, elevation, orientation, etc., at a given location. Section 4 provides details about the test cases. The procedure is defined and validated by using the observed IR_1, in four different study areas: the Liguria region, the Piedmont region, and the northern and southern French Alps, which are characterized by different H_d regimes (Parodi and Boni 2001; Boni and Parodi 2002; Boni et al. 2006). Results are provided in section 5 and discussed in section 6. Conclusions are provided in section 7.

2. Definition of the set of descriptors

The occurrence of extreme rainfall over complex orography is often associated with a combination of synoptic, mesoscale, and microphysics ingredients. Sawyer (1956) suggests that the amount and distribution of orographic rain, at the event scale, can be explained by considering meteorological processes on three different spatial scales.

- First, synoptic factors determine the characteristics of the air mass that is crossing the hills (i.e., its wind speed and direction, as well as its stability and humidity).
- Second, the dynamics of air motion over and around hills determines the depth of the airmass layer affected by the uplift.
- Third, the microphysics of clouds and rain determines the amount and the state of the water that reaches the ground.

Barros and Kuligowski (1998) studied the evolution of precipitation features during a severe wintertime rainfall and flooding event associated with a cold front, which crossed the central Appalachians, through the analysis of radiosonde, rainfall, and streamflow gauge data and the Weather Surveillance Radar-1988 Doppler (WSR-88D) images. Their work provides striking evidence of a linkage between heavy precipitation cells and orography at the event scale.

Lin et al. (2001) synthesized, again at the event scale, a few common synoptic and mesoscale scenarios prone to heavy orographic rainfall on the basis of the study of some U.S., Alpine, and East Asian test cases. They singled out the following common synoptic and mesoscale ingredients leading to heavy orographic rainfall: 1) conditionally or potentially unstable airstream impinging on the mountains, 2) a low-level jet stream, 3) a steep mountain, and 4) a quasi-stationary synoptic system slowing down the convective system over the threatened area.

Rudari et al. (2004) found that extreme rainfall in northwestern Italy is produced by a few easily identifiable large-scale meteorological patterns associated to the orographic uplift of moist air.

So far, several theories of orographic precipitation, often relying on the simple synoptic, mesoscale, and microphysical ingredients outlined before, have already been proposed in literature: from the early works of Hobbs et al. (1973), Collier (1975), and Smith (1979), which introduced the idea of upslope model, to the more recent linear theory of Smith and Barstad (2004) and Barstad and Smith (2005), which extends that formulation by including airflow dynamics, condensed water, and downslope evaporation.

According to these theories, rainfall amounts $R_d(\mathbf{x}, t)$, in a generic location, depend, at the event scale, on several topographic and meteorological factors. Meteorological factors are those that introduce time dependence for $R_d(\mathbf{x}, t)$. They are large-scale wind velocity (at 700 hPa) of magnitude U and direction α, $(U, \alpha) = \mathbf{U}(\mathbf{x}, t)$ (Holton 2004), stability frequency $N(\mathbf{x}, t)$, the characteristic time scale for cloud water conversion into hydrometeors $\tau_c(\mathbf{x}, t)$, and the characteristic time scale for hydrometeor fallout $\tau_f(\mathbf{x}, t)$.

Studying the interactions between moist airflow dynamics and relief, Smith and Barstad (2004) found that the role of the relief height Z can be summarized in the nondimensional mountain height, $M = ZN_m/U$, where N_m is the moist stability frequency. For $M < 1$ the moist air will flow over the relief and the forced ascent process is very efficient, conversely the moist air will flow around the hill and flow splitting will result. Reasonable parameter values for the Alpine region are $U \approx 10\ \mathrm{m\,s^{-1}}$ and $N_m = 0.0025$–0.005 s (Buzzi and Foschini 2000; Barstad and Smith 2005; Smith et al. 2003). The height threshold for forced ascent results in $Z_t = 2000$–4000 m and suggests the relevance of a relief height $Z(\mathbf{x}, t)$ parameter over the whole Alpine area. The importance of the horizontal scale of orography $L(\mathbf{x})$ (interpreted as the distance from floodplain/coastline) and local slope $S(\mathbf{x})$ was underlined by Jiang (2000, 2003) and Smith and Barstad (2004). When $L(\mathbf{x})$ increases, the vertical motion penetrates more deeply into the atmosphere thus increasing the condensation efficiency. Furthermore, as the scale increases, more condensed water is able to convert into hydrometeors and to fall out, before being carried to the leeside region of descent, thus increasing the precipitation efficiency. Such consideration supports the choice of $L(\mathbf{x}, \overline{\alpha})$ as the relevant regression parameter and its evaluation along the dominant wind direction $\overline{\alpha}$.

The relevant effect of mountain slope $S(\boldsymbol{x}, \overline{\alpha})$, evaluated along the dominant wind direction, on the precipitation spatial distribution has been validated by several studies (Spreen 1947; Smith 1979; Barros and Lettenmaier 1993; Daly et al. 1994; Roe 2005).

We can summarize all the reported results with the following expression:

$$R_d(\mathbf{x}, t) = \ldots = f[Z(\mathbf{x}), S(\mathbf{x}, \overline{\alpha}), L(\mathbf{x}, \overline{\alpha}), \mathbf{U}(\mathbf{x}, t), N(\mathbf{x}, t), \tau_c(\mathbf{x}, t), \tau_f(\mathbf{x}, t)] + \epsilon(\mathbf{x}, t). \quad (3)$$

The error term $\epsilon(\mathbf{x}, t)$ accounts for the second-order effects due to neglected parameters. Therefore, the orographic precipitation can be considered as a function of three groups of ingredients: large-scale uphill-directed flow containing enough water to easily reach saturation, dynamics determining the pattern of vertical motion over the topography, the condensation processes and microphysics involving the conversion of condensate into hydrometeors, and the subsequent falling of the hydrometeors to the ground. When annual maximum values of $R_d(\mathbf{x}, t)$, evaluated according to Eq. (2), are of concern, we can reasonably assume that $\mathrm{IR}_d(\mathbf{x}, t) = E[H_d(\mathbf{x}, t)]$ depends on the climatologic values of the variables in (3), therefore time dependence disappears. In this framework, the interannual and decadal variability in hydrometeorological regimes controlling extreme events has been ignored due to the limited extension in time of the samples, whose duration, though considerable when compared to those of other regions, is too limited to allow here any reliable conclusion on multiannual variability (Frei et al. 2000; Frei and Schar 2001).

Meteorological factors affecting expression (3) deserve a separate discussion when IR_d are considered. A regional frequency analysis in Alpine regions singles out homogeneous regional areas whose size rarely exceeds 10^4–10^5 km^2. Climatic studies performed by Frei and Schar (1998), Frei et al. (2000), and Rudari et al. (2005) demonstrate that climatological values of $\mathbf{U}$, N, τ_c, and τ_f related to extreme rainfall events have spatial scales of variability of about one order of magnitude larger than the dimension of the homogeneous regions detected in mountainous areas. Therefore, since an analysis is performed for each homogeneous region, we assume that $\mathbf{U}$, N, τ_c, and τ_f do not affect the spatial variability of IR_d. However, the climatological value of large-scale wind direction, $\overline{\alpha}$ cannot be neglected, since it affects the values of $S(\mathbf{x}, \overline{\alpha})$ and $L(\mathbf{x}, \overline{\alpha})$, as "seen" by the air flux. We propose for IR_d the following general expression:

$$\mathrm{IR}_d = f[Z(\mathbf{x}), S(\mathbf{x}, \overline{\alpha}), L(\mathbf{x}, \overline{\alpha})] + \epsilon'(\mathbf{x}). \quad (4)$$

Therefore, we assume that $Z(\mathbf{x})$, $S(\mathbf{x}, \overline{\alpha})$, $L(\mathbf{x}, \overline{\alpha})$, and $\overline{\alpha}$ compose the most general set of variables describing IR_d spatial variability. The functional form of Eq. (4) has to be investigated. In it no hypothesis about the form of the dependence of IR_d on the selected set of variables is made. By examining the Smith and Barstad (2004) advection-convection model, a linear dependency of the source of condensed water on $Z(\mathbf{x})$, $S(\mathbf{x}, \overline{\alpha})$, and $L(\mathbf{x}, \overline{\alpha})$ can be assumed.

Here, we extend the linear dependency to rainfall and assume a linear form for Eq. (4):

$$\mathrm{IR}_d(\mathbf{x}, \alpha) = \beta_Z Z(\mathbf{x}) + \beta_S S(\mathbf{x}, \overline{\alpha}) + \beta_L L(\mathbf{x}, \overline{\alpha}) + \gamma. \quad (5)$$

The method can be further generalized, without any loss of its robustness and transferability, by adding other variables to the general set [e.g., for areas where neglected meteorological variables appearing in Eq. (3) show significant variability in the homogeneous region]. In this case, the method is complicated by the need to have climatological values of the variables for each gauged site.

3. Estimating topographic parameters

The relevant variables affecting IR_d and singled out in Eq. (5) call for a general procedure to filter out local topographic parameters.

The analysis of rain gauge data performed by Frei and Schar (1998) to map the mean patterns of annual, seasonal, and monthly precipitation over the Alps shows the presence of relevant peaks of rainfall accumulation over the southern slopes with a spatial scale much smaller than the entire Alpine massif, even though much larger than individual river valleys. This suggests that small-scale orographic features do not greatly affect mean rainfall spatial patterns. The filtering procedure must, therefore, be able to extract large-scale features of orography, containing higher morphological information, while neglecting small-scale perturbations. According to Sawyer (1956), such a procedure should describe to some extent how the air mass "sees" the relief structures and, therefore, how the dynamics of the air motion is on average affected by orography. Here we propose a filter, when applied to a DEM, which filters out features that produce second-order effects on rainfall. The filtering procedure proposed is based on a 2D Fourier series analysis of orography.

The Fourier transform is a linear operator that maps functions to other functions. Broadly speaking, the Fourier transform decomposes a function into a continuous spectrum of its frequency components, while the inverse transform synthesizes a function from its spectrum of frequency components. By defining $z(\mathbf{x})$ the elevation at a generic location $\mathbf{x} = (x, y)$, its discrete Fourier transform P is given by the following equation:

$$P(i, j) = \frac{1}{MN} \sum_{x=0}^{M-1} \sum_{y=0}^{N-1} z(x, y) \exp\left[-2\pi i \left(\frac{ix}{M} + \frac{jy}{N} \right) \right]. \quad (6)$$

The numbers $M = M_1$ and $N = N_1$ of the components are analyzed to evaluate those that include, in the power spectrum $\mathrm{PS} = P \times \mathrm{conj}(P)$, the higher "energy" content, interpreted here as "morphological" information content. The inverse discrete Fourier transform is applied to the M_1 and N_1 components only and the filtered DEM is obtained by converting back to the spatial domain:

$$z_f(x, y) = \frac{1}{M_1 N_1} \sum_{u=0}^{M_1-1} \sum_{v=0}^{N_1-1} P(i, j) \exp\left[2\pi i \left(\frac{ix}{M_1} + \frac{jy}{N_1} \right) \right], \quad (7)$$

where z_f represents the filtered orography.

From the filtered DEM, the parameters $Z(\mathbf{x})$, $L(\mathbf{x}, \overline{\theta})$, and $S(\mathbf{x}, \overline{\theta})$ at a given location $\mathbf{x}_0$ are extracted as follows:

$$\begin{aligned} Z(\mathbf{x}_0) &= z_f(\mathbf{x}_0) \\ L(\mathbf{x}_0, \overline{\theta}) &= |\mathbf{x}_0 - \mathbf{x}_{\min}| \\ S(\mathbf{x}_0, \overline{\theta}) &= \nabla z_f(\mathbf{x}_0) \cdot \mathbf{D}(\overline{\theta}) \\ x_{\min} | z_f(\mathbf{x}_{\min}) &= 0 \text{ m (coastline)} \\ x_{\min} | z_f(\mathbf{x}_{\min}) &= 500 \text{ m (floodplain)} \\ \mathbf{D}(\overline{\theta}) &= (\cos\overline{\theta}, \sin\overline{\theta}). \end{aligned} \quad (8)$$

4. The case studies

a. Datasets

The methodology outlined in the previous section has been applied to sample IR_d for $d = 1$ h (IR_1 in the following). Values have been estimated by using the sample mean of H_1 recorded at gauged sites. The study region is shown in Fig. 1. The observed H_1 were provided for Liguria and Piedmont by the Italian Hydrological Service, for the French Alps by the Electricité de France (EDF), Météo France, the Service Régional d'Aménagement des Eaux (SRAE), the Institut de Recherche pour l'Ingenierie de l'Agriculture et de l'Environnement (CEMAGREF), and the Direction Departementale de l'Equipement et de l'Agriculture du Cher (DDAF). The number of rain gauge sites considered varied from region to region: 89 for Liguria, 67 for Piedmont, 47 for the southern French Alps, and 49 for the northern French Alps. The record length N_i for each rain gauge site varied from 10 to 66 yr.

Moreover, the high density of the rain gauges network available in this study (on average a rain gauge every 50 km^2) allowed the provision of reliable estimates of the regression parameters relevant for the mapping of the rainfall index in ungauged sites. In particular, according to the Nyquist frequency, the adopted network allowed an approximate 30–40-km minimum

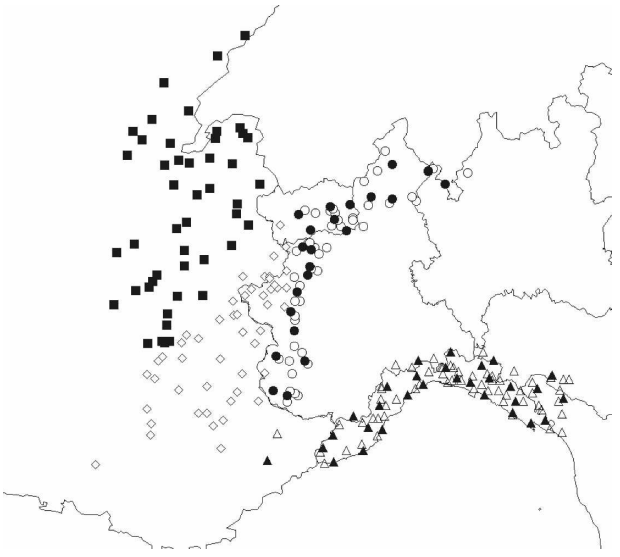

FIG. 1. Orography of the region where the analyzed H_d were collected and location of the rain gauges. Different symbols correspond to different regions where the analysis has been carried out: triangle = Liguria (white for calibration, black for validation); circle = Piedmont (white for calibration, black for validation); black square = northern French Alps; and white diamond = southern French Alps.

spatial-scale resolution. Consequently, albeit crudely, the smaller scales of orography can be resolved and there is ground to state that smaller scales are not relevant, as demonstrated in this study. It is worth mentioning once more how this study area provides one of the more dense networks in regions of complex terrain that one can find around the world.

For Liguria and Piedmont the high number of stations also allowed the identification of two subsets for calibration and validation. For Liguria, 59 stations were used for calibration and 30 for validation. For Piedmont, 45 stations were used for calibration and 22 for validation (see Fig. 1).

The four regions here considered correspond to the "homogeneous regions" discussed elsewhere. Region borders have been defined according to the main orientation of mountain slopes and valleys and to the prevalent airflow regimes during extreme events. Homogeneity tests were performed following the hierarchical procedure proposed by Fiorentino et al. (1987) and Gabriele and Arnell (1991), based on the assumption of the Two Component Extreme Value (TCEV; Fiorentino et al. 1987) distribution as nondimensional cumulative density function (CDF) for IR_1 in homogeneous regions. The TCEV model can be interpreted as the CDF of the annual maximum for a Poissonian process composed of a mixture of two independent populations, each one of them described by an exponential distribution. One population was named the ordinary component and represents the H_d values that occur more frequently. The other was named the extraordinary component and represents the population that includes the outliers. The analytical expression of the CDF for the TCEV distribution is

$$F_{H_1}(h_1') = \exp\left[-\Lambda_1 \exp(-\eta h_1') - \Lambda_* \Lambda_{\theta_*}^{\frac{1}{\theta_*}} \exp\left(-\eta \frac{h_1'}{\theta_*}\right)\right], \tag{9}$$

where $h'_1 = h_1/\mathrm{IR}_1$, η is the so-called shape parameter and h_1 is the recorded value of the annual rainfall maximum for $d = 1$ h. The parameters Λ_* and θ_* are defined as $\theta_* = (\theta_2/\theta_1)$ and $\Lambda_* = (\Lambda_2/\Lambda_1^{(1/\theta_*)})$; Λ_i ($i = 1, 2$) represents the annual expected number of H_1 realizations belonging, respectively, to the ordinary and the extraordinary component, and θ_i ($i = 1, 2$) represents the expected value of the two populations.

The testing procedure assumes that parameters related to higher-order moments have less spatial variability. Consequently, it evaluates Λ_*, θ_*, which define the coefficient of skewness (CS) on larger regions and then Λ_1, related to the coefficient of variation (CV) on the same or smaller subregions (Gabriele and Arnell 1991). Then, the observed sample frequency distributions of CS and CV in the region, hypothesized as homogeneous, is compared to the correspondent probability distributions obtained through a Monte Carlo generation based on the CDF in (9). If they match, the region is assumed as statistically homogeneous. Results for the whole study area are reported in Tables 1 and 2. They show that the χ^2 tests between sample and theoretical probability distributions have positive results, therefore the regions can be assumed as homogeneous.

b. Dominant wind directions

In this study, in accordance with the usual convention, wind direction is defined by clockwise degrees starting with the 0° at north. To estimate the value of the dominant wind direction, $\bar{\alpha}$, during intense rainfall events, an analysis of air motion and precipitation growth in the different homogeneous regions is presented below.

In the case of Liguria and the southern French Alps, heavy precipitation events occur during the fall season (Boni et al. 2006; Mertz 1957; Tibaldi and Buzzi 1983; Tibaldi and Molteni 1990) and are typically associated with a baroclinic trough approaching the region from the west, which promotes a southerly low-level advection of moisture impinging toward the Ligurian Apennines and Alps. The climatological analysis of wind per-

TABLE 1. Regional frequency analysis, first level. Results of the homogeneity tests. The χ^2 test on sample and theoretical CDFs for CS passes for each region.

Region	Λ_*	θ_*	Sample CS		Generated CS		Degree of freedom (n)	χ^2	$\chi^2_{\alpha=0.05,\, n-3}$
			Std dev	Mean	Std dev	Mean			
Liguria	0.50	1.48	0.66	1.01	0.64	1.01	16	9.66	22.4
Piedmont	0.19	1.78	0.77	1.04	0.70	1.09	13	13.16	18.30
Southern Alps	0.23	2.54	0.83	1.44	0.86	1.31	10	8.12	14.2
Northern Alps	0.24	2.38	0.76	1.21	0.83	1.22	9	11.9	12.60

formed by Castino et al. (2003) showed that in such area the most frequent low-level wind direction is southwesterly oriented. For the analysis, we used values of $\bar{\alpha}$ ranging between the interval $30° \leq \bar{\alpha} \leq 60°$ in accordance with the aforementioned convention.

Over the Piedmont area, the precipitation is most intense when the mean geostrophic flow is southerly or southeasterly impinging against the Alpine barrier, as shown by the analysis of the 1994 and 2000 floods in Piedmont and of some Mesoscale Alpine Programme (MAP) 1999 events (Buzzi and Foschini 2000; Ferretti et al. 2000; Houze et al. 2001; Massacand et al. 1998; Rotunno and Ferretti 2001). Values of $\bar{\alpha}$ around 330° are, then, the most probable.

In the northern French Alps area, the quasi-stationary northwest cyclonic regime is dominant (Mertz 1957; Schiesser et al. 1995) and promotes the highest precipitation amount during the main convective period (May–September; Frei and Schar 1998). Frontal structures associated with depressions centered over northern Europe tend to move in from west and northwest and the presence of the Alpine barrier can trigger strong convective episodes embedded in the frontal zone (Blanchet 1990). Values of $\bar{\alpha}$ range from 105° to 135°.

5. Results

a. DEM filtering

To define the optimal number of components of the DEM Fourier transform in (6) to be used, we first analyzed wavelengths that preserved more than 80% of the morphologic content. In Fig. 2, we show that the spectral components of wavelength larger than 100 km already describe more than 80% of the spatial variability. We, then, truncated the Fourier transform in (6) in order to obtain a filtered DEM using wavelengths larger than 200, 100, and 50 km that described the 80%, 90%, and 95%, respectively, of the observed orographic spatial variability (Fig. 3). These three filtered DEMs z_{f80}, z_{f90}, and z_{f95} are the starting point from which to evaluate the independent variables of the regression in (5). A least squares linear regression is performed for each of the three cases, using the general set of variables S, Z, and L, evaluated through Eq. (5), for values of $\bar{\alpha}$ around dominant wind directions as defined in the previous paragraph.

b. Methodological approach for the model evaluation

The results of the application of Eq. (5) are reported in the following paragraphs for the four homogeneous regions considered.

The t statistic is applied on each coefficient of regression in order to test the significance of the dependence of IR_1 on each of the variables of Eq. (5). This allows us to identify the optimal subset of variables that describe the IR_1 spatial variability.

The F test is performed in order to assess whether or not the chosen form of the model (linear in this case) is appropriate for Eq. (5). It is a statistic test commonly used to decide whether a model, as a whole, has statistically significant predictive capability, considering the number of variables necessary to achieve it.

TABLE 2. Regional frequency analysis, second level. Results of the homogeneity tests. The χ^2 test on sample and theoretical CDFs for CV passes for each region.

Region	Λ_1	Sample CV		Generated CV		Degree of freedom (n)	χ^2	$\chi^2_{\alpha=0.05,\, n-4}$
		Std dev	Mean	Std dev	Mean			
Liguria	15.75	0.075	0.40	0.067	0.39	16	20.36	21.02
Piedmont	19.55	0.076	0.39	0.07	0.38	13	9.81	16.91
Southern Alps	31.66	0.101	0.41	0.10	0.39	10	12.4	12.6
Northern Alps	39.02	0.102	0.37	0.096	0.36	9	2.97	11.07

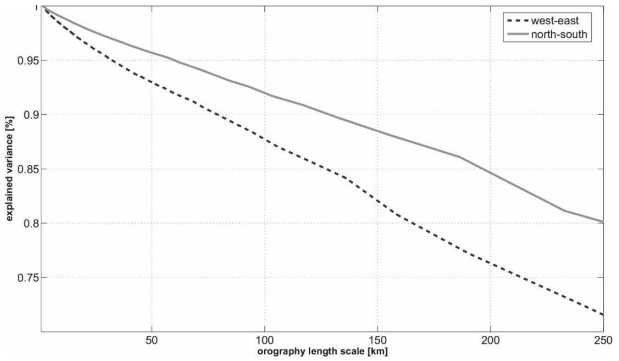

FIG. 2. The explained variance of the DEM power spectrum depends on the orography wavelength considered. Longer wavelengths explain less variance and provide a smoother description of orography.

The Durbin–Watson test is used to verify whether the residuals of the linear multiple regression are independent (Durbin and Watson 1950). This test is among the most widely applied in time series analysis and is based on the assumption that the errors in the regression model are generated by a first-order autoregressive process observed at equally spaced time periods.

In the case of the Piedmont and Liguria regions, where a larger number of stations are available, the linear regression equation were both calibrated and validated by splitting the dataset into two subsets. The calibration set included data recorded at 59 stations for Liguria and 45 stations for Piedmont, the remaining 30 (Liguria) and 22 (Piedmont) were used for validation.

Validation was performed by applying the regression coefficients to IR_1 estimated for the validation set and then by comparing differences between observed and predicted values with the $100(1 - \alpha)$ confidence interval on the prediction of future values. The interval, following Kottegoda and Rosso (1997), was evaluated by the following expression:

$$\Pr\Big\{E[\mathrm{IR}_{d=1}] - t_{n-p,\alpha/2}\sqrt{\sigma^2[1 + \mathbf{a}(\mathbf{X}^{\mathrm{T}}\mathbf{X})^{-1}\mathbf{a}^{\mathrm{T}}]} < \mathrm{IR}_{d=1} < \quad \ldots$$
$$\ldots < E[\mathrm{IR}_{d=1}] + t_{n-p,\alpha/2}\sqrt{\sigma^2[1 + \mathbf{a}(\mathbf{X}^{\mathrm{T}}\mathbf{X})^{-1}\mathbf{a}^{\mathrm{T}}]}\Big\} \quad \geq 1 - \alpha, \tag{10}$$

where t is the t statistic, n is the number of predicted variables, and $\mathbf{X}(n \times p)$ is the matrix containing the values of the $p - 1$ explanatory variables at the observation points plus a column of 1s to cater to the constant γ. We assume here $\alpha = 0.05$.

c. The Liguria region

1) CALIBRATION

For the Liguria region, the synthetic relief descriptors used in Eq. (5) were evaluated along different dominant wind directions, ranging from 30° to 60°. This range presented the most frequently observed low-level wind directions in all the regions (see section 4). A total of 59 randomly chosen and spatially homogeneously distributed rain gauge sites were used to calibrate the proposed model (see Fig. 1). The choice of the level of filtering and of the wind direction $\overline{\alpha}$ was performed by maximizing the coefficient of multiple determination R^2 of the linear regression in (5). An 80% variance DEM was identified as the one that maximized, for all wind directions, the R^2 (see Fig. 4). Table 3 shows the results of the trivariate least squares linear regression performed for the wind direction $\overline{\alpha} = 60°$, which maximized the value of R^2. In this case we have both the highest values of F and R^2. In particular, $R^2 \simeq 0.60$ means that about 60% of the variation in IR_1 is explained by the trivariate linear regression model. The F test confirms that the linear regression model adequately describes the functional relation between IR_1 and the chosen variables. The t test results in Table 3 show that, for a level of significance $\alpha = 0.05$ and for $\overline{\alpha} = 60°$, the slope $S(\mathbf{x}, 60°)$ is the most important parameter in the linear regression, while the dependence on the distance from the coastline is negligible. The distance from the coastline can be retained as prediction, but its contribution to the linear regression is negligible. Consequently for a homogeneous region like Liguria the optimal subset of regression variables is given by slope and distance from the coastline.

2) VALIDATION

The remaining 30 gauged sites in the Liguria region were used to validate the model. The model prediction at the gauge location was compared to observations of IR_1. Figure 5 suggests that the results are satisfactory, since almost all the predicted values (28 of 30) are in the 95% confidence interval defined by (10). The bias, as a measurement of sign and magnitude of the mean errors, and the mean absolute error (MAE), as a precision measurement, were computed. The values found (bias = 0.4 mm and MAE = 5.2 mm) were lower than those usually found in literature (Basist and Bell 1994; Daly et al. 1994; Marquinez et al. 2003), even if these studies refer to mean annual and monthly pre-

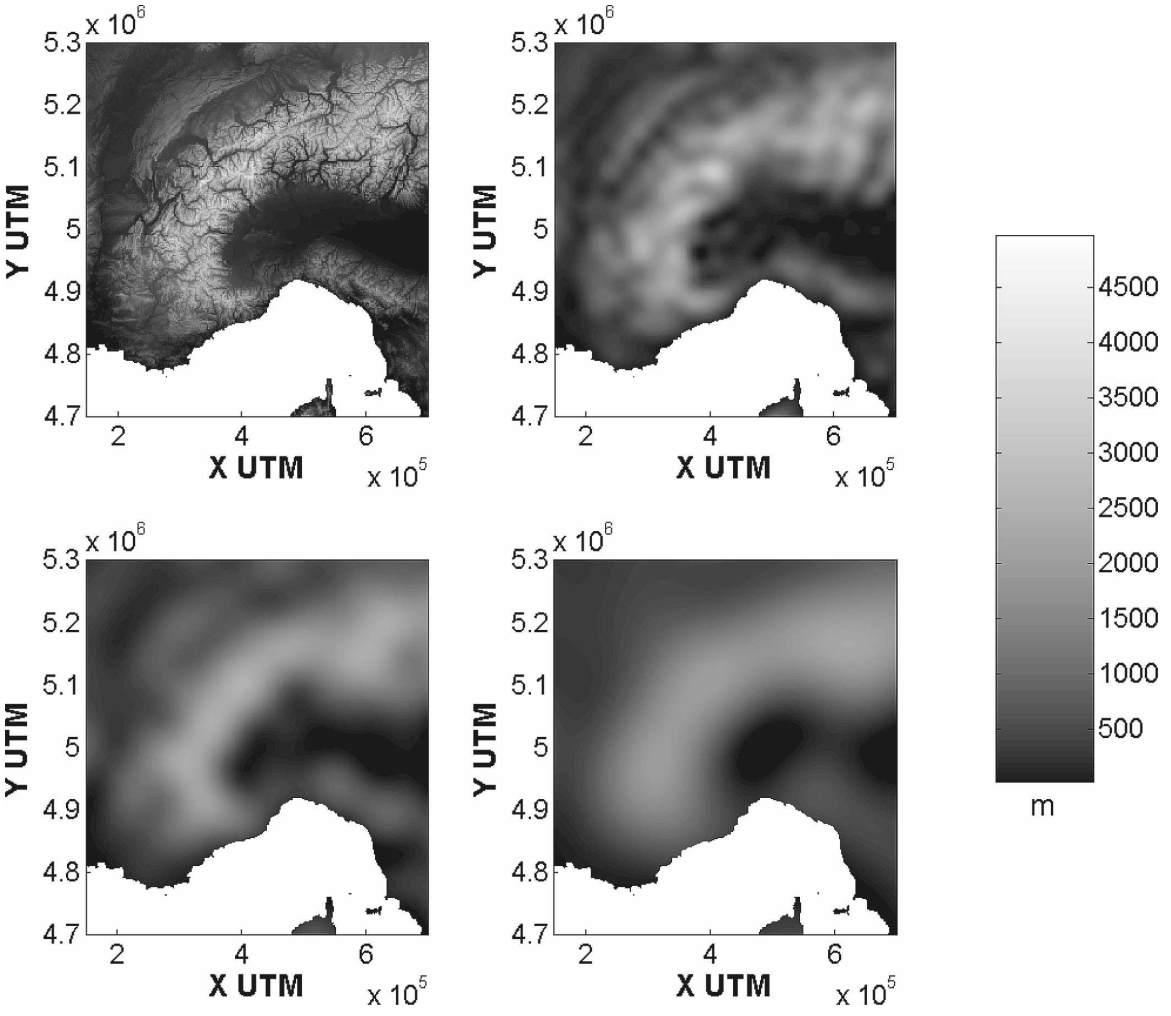

FIG. 3. Comparison between (top left) unfiltered DEM, (top right) 95% variance DEM, (bottom left) 90% variance DEM, and (bottom right) 80% variance DEM.

cipitation. The regression residuals $r_i = (e_i/\sigma_e\sqrt{1 - h_{jj}})$ (where e_i is the model error for the ith observation, h_{jj} are the diagonal elements of the hat matrix $\mathbf{H} = \mathbf{Y}(\mathbf{Y}' \cdot \mathbf{Y})^{-1}\mathbf{Y}'$, and $\mathbf{Y} = [Z, S, L]$) were normally distributed and uncorrelated, as shown in Table 4 by the results of the Kolmogorov–Smirnov and Durbin–Watson tests.

The index rainfall map that was estimated by using the optimal subset of regression variables is shown in Fig. 6. The estimates can be placed in the right drainage basin since the regression variables are a function of the localization.

d. The Piedmont region

1) CALIBRATION

For this region the set of synthetic relief descriptors was computed along wind direction $\overline{\alpha}$, which ranged

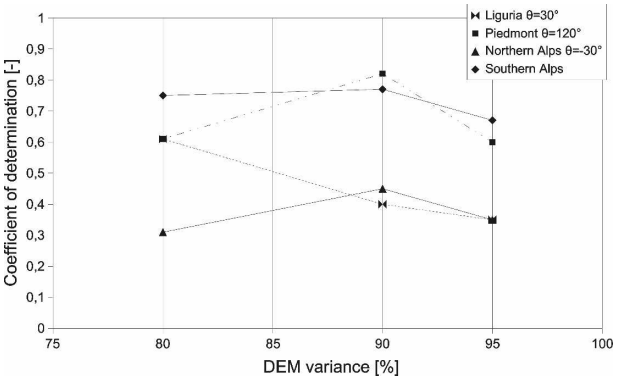

FIG. 4. Coefficient of multiple determination R^2 for the regression in Eq. (5). Results for low-level wind direction that maximize the values R^2 for each region are reported.

TABLE 3. Results and statistics of the linear regression of $IR_{d=1}$ vs synthetic relief descriptors for the four study regions. The θ values are those that maximize R^2.

Region	Liguria	Piedmont	Southern Alps	Northern Alps
θ (°)	60	330	60	120
R^2	0.61	0.82	0.77	0.45
F	28.7	57.9	51.5	10.9
$F_{\alpha=0.05}(k, n-k-1)$	2.76	2.83	2.81	2.82
$n-k-1$	55	41	45	43
γ (mm)	44.3	37.4	28.8	21.9
$\lvert t_\gamma \rvert$	15.2	16.8	23.6	22.3
β_z (m^{-1})	−0.02	−0.011	−0.007	-8.6×10^{-3}
$\lvert t_{\beta_Z} \rvert$	3.0	11.8	6.79	2.46
β_s (–)	904	132.6	−40.7	164
$\lvert t_{\beta_S} \rvert$	4.1	2.63	1.36	6.79
β_L (km^{-1})	-7.5×10^{-3}	5×10^{-4}	-5×10^{-4}	−0.08
$\lvert t_{\beta_L} \rvert$	0.10	0.02	0.07	2.33
$t_{\alpha=0.05}(k, n-k)$	1.68	1.68	1.68	1.68

from 300° to 345° counterclockwise in the west–east direction, which is representative of the typical propagation direction of extreme events affecting this area (see section 4). The calibration set in this case included 45 rain gauges (see Fig. 1).

The 90% variance DEM, filtering out the orography wavelengths lower than about 100 km, maximized R^2 values for all wind directions (Fig. 4) and was adopted for the estimation of the parameters of Eq. (8). When compared with the Liguria region, the processes responsible for spatial variability of IR_1 in Piedmont seem to be sensitive to finer orographic details. This can be explained by looking again at Fig. 3. The morphology of the mountain chain in Liguria is relatively simple when compared to the orography of Piedmont as it is almost a single wave from the sea to the floodplain. Thus, a 90% variance DEM (bottom-left panel) does not add, for Liguria, any significant detail of mountain shape to those given by the 80% variance DEM (bottom-right panel). In Piedmont, the presence of many long valleys variously oriented and the relative effects on shading and slopes must be described and it cannot be done by using the 80% variance DEM. The results reported in Table 3 are for the flow direction $\overline{\alpha} = 330°$ that maximized R^2. The R^2 values were high, around 0.8. The orography and an average low-level wind direction can be assumed here to be responsible for the amount of rainfall produced during extreme events. The t statistic shows that, for the level of significance $\alpha = 0.05$ and $\alpha = 330°$, the altitude Z is the dominant parameter in the linear regression, while the role of the distance L from the floodplain is still negligible. Therefore, for this region the optimal subset of regression variables includes the aforementioned height Z and the slope S. This result confirms that for the Piedmont region the orographic shielding effect is the dominant explanatory factor in the linear regression and is responsible for comparatively large-scale atmospheric ascent and enhanced precipitation.

2) VALIDATION

The positive behavior of the model, shown in the previous paragraph, is also confirmed by the validation summarized in Fig. 7: 21 of 22 values are included in the 95% interval of prediction of future values. The bias = −0.27 mm and the MAE = 3.2 mm are even lower than in the case of Liguria. The testing of the gaussianity and the uncorrelation on t_i reported in Table 4 was success-

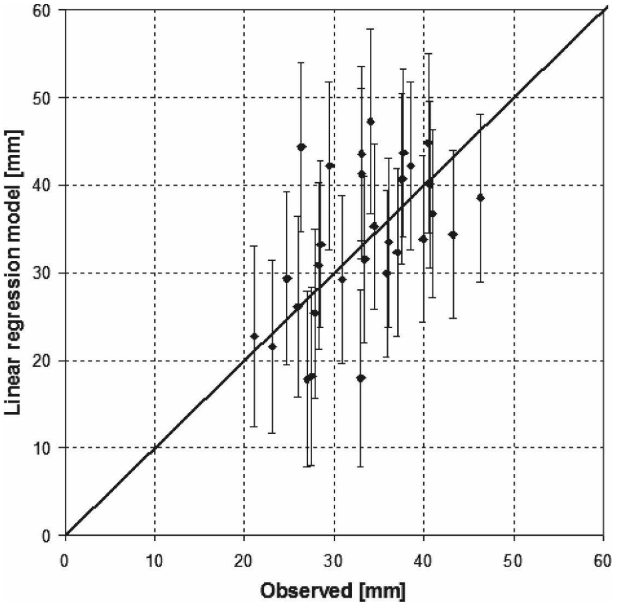

FIG. 5. Comparison between observed and modeled $IR_{d=1}$ for 30 randomly chosen rain gauge stations (Liguria region). The prediction interval for a future value of $IR_{d=1}$ is shown ($\alpha = 0.05$).

TABLE 4. Results of the Durbin–Watson test and Kolmogorov–Smirnov test for level of significance $\alpha = 0.05$.

Region	Hypothesis t_i: $N(0, \sigma_t)$		Residual correlation		
	Kolmogorov–Smirnoff test		Durbin–Watson test		
	t_{max}	$t_{\alpha=0.05}$	Observed value	Limits $\alpha = 0.05$	n
Liguria	0.069	0.177	1.90	1.50–2.50	59
Piedmont	0.067	0.202	1.85	1.65–2.35	45
Southern France	0.07	0.198	2.30	1.65–2.35	49
Northern France	0.132	0.194	1.70	1.65–2.35	47

ful. Once more the Kolmogorov–Smirnov and Durbin–Watson tests suggest that the residuals from the linear multiple regression are also independent for the Piedmont region.

e. Southern French Alps region

For this study region, due to a lack of rain gauges, only the calibration was performed. Analysis demonstrated that, as like Piedmont, the 90% variance DEM, filtering out the orography wavelengths lower than about 100 km, guarantees the highest R^2 (Fig. 4). However, the direction of propagation of extreme events seems to play a marginal role in the trivariate linear regression, since values of R^2 for any considered low-level climatological wind direction ($30° \leq \overline{\alpha} \leq 60°$) are nearly coincident. This result was also confirmed by the statistics shown in Table 3: the optimal subset of regression variables was reduced to the height $Z(\mathbf{x})$ in agreement with the findings of the gradex method proposed by Bouvard and Garros-Berthet (1994). An indirect validation of the model was carried out by analyzing the regression residual t_i. As in the case of the other regions considered in this study, the residuals t_i do not exhibit any trend along the whole model prediction range. On the basis of the Kolmogorov–Smirnov and Durbin–Watson tests, they were normally distributed and they did not present any degree of autocorrelation as suggested by test results shown in Table 4. Figure 8 shows the map of the IR_1, for the southern French Alps region, estimated by using the optimal subset of regression variables.

f. Northern French Alps region

For this study region, the 90% variance DEM guaranteed the highest R^2, even though in this case the performances of the multivariate linear regression model were worse than the other areas considered in this study (Fig. 4). In respect to the 90% variance DEM, the regression statistics showed that all the synthetic relief descriptors contributed to explain the spatial variability of IR_1 with a slight predominance of the elevation. Moreover, the best results were obtained for wind di-

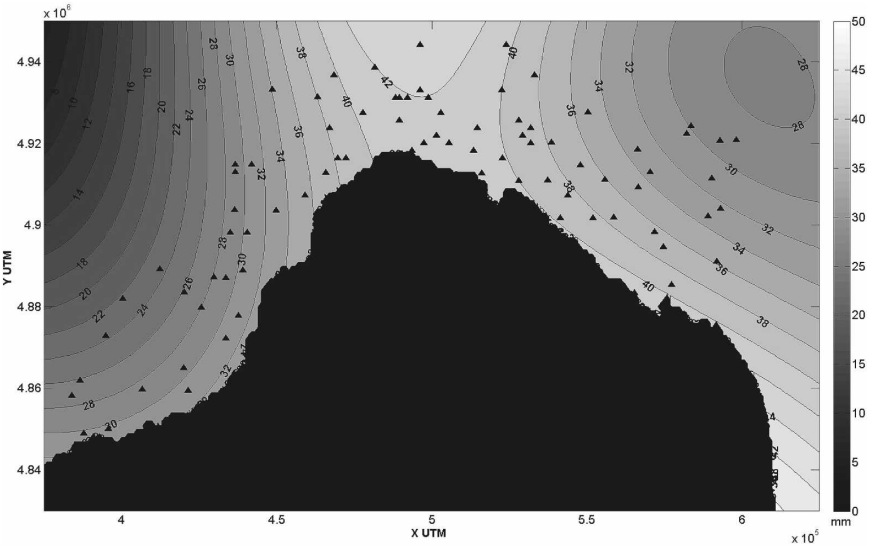

FIG. 6. Contour lines of IR_1 for the Liguria region.

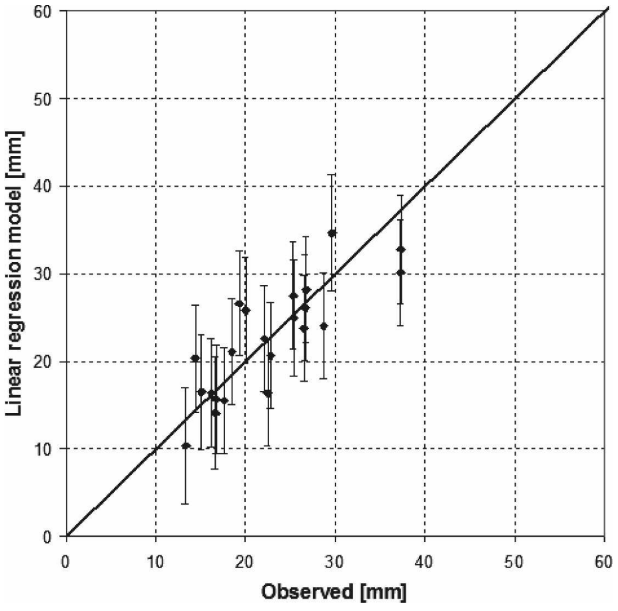

FIG. 7. Comparison between observed and modeled IR_1 for 22 randomly chosen rain gauge stations (Piedmont region). The prediction interval for a future value of IR_1 is shown ($\alpha = 0.05$).

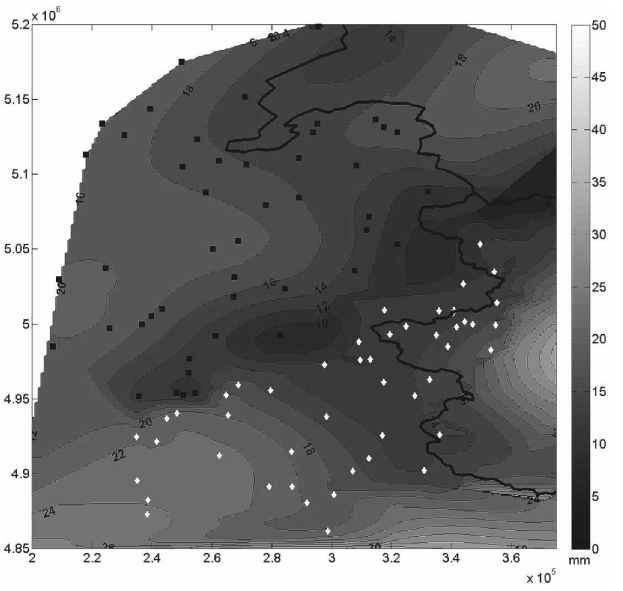

FIG. 8. Contour lines of IR_1 for the northern and southern French Alps regions.

rections around 120° showing both the highest values of F and R^2. The residuals, also for this region, did not present any systematic pattern in respect to the independent variables, as confirmed by the results of Table 4 and in particular by the Durbin–Watson test. The Durbin–Watson test statistic is designed to detect errors that follow a first-order autoregressive process. This statistic also plays an important role as a general test of model misspecification. Figure 8 shows the IR_1 map, for the northern French Alps region, estimated by using the optimal subset of regression variables. The northern French Alps region is characterized by values of index rainfall lower than those estimated in the southern part.

6. Discussion

Besides the satisfactory performance of the proposed mapping method, the main result of this study appears to be that the relevant wavelength of orography for spatial variability of mean hourly annual rainfall maxima is about 100 km and that both the slope and elevation are the most important predictors in the four case studies.

The broad horizontal wavelength obtained apparently contrasts with many statistical studies of rainfall spatial variability that identify scales less than 10 km as appropriate. However, it is worth pointing out some differences in those studies with respect to this paper.

First, this research did not intend to study the spatial variability of intense rainfall at the event scale, seen as a single realization of the rainfall stochastic process, but instead dealt with the mapping of the rainfall index defined as the mean of hourly annual rainfall maxima. In the case of deep convective processes at the event scale, finescale orography details can trigger the rainfall event and can deeply affect its resulting spatial pattern (see studies related to the MAP project), but when we focus on the mean value of hourly annual rainfall maxima, it is reasonable to expect that the relevant scales of orography are smoother and wider.

Second, while other studies referred to spatial patterns of average rainfall accumulated over long time windows (i.e., day, month, and season), we addressed the mapping of IR_1, which is annual rainfall maxima for a short duration ($d = 1$ h).

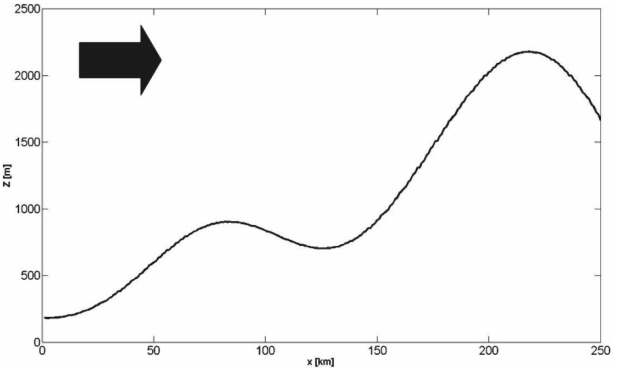

FIG. 9. Sections of the smoothed orography for northern France along the dominant wind direction. The black arrow indicates the direction of the incoming wind.

Third, other studies (Hutchinson and Bischof 1983; Hutchinson 1998; Sharples et al. 2005) mainly considered areas (like Australia) characterized by a climatology and orography quite different from that typical of the four homogeneous regions that we analyzed.

Finally, they identified the optimal spatial scale of the interaction between precipitation and topography by looking for the minimum of a generalized cross validation function (GCV; Sharples et al. 2005). However, this minimum is, often, not very strong and the difference between the value of GCV for scale values equal to 10 or 100 km (and higher) is very small. Consequently, the identification of the optimal scale is often not unambiguous.

Therefore, it is interesting to interpret the results obtained in the previous section and the dominant role of predictors like slope or elevation referring to the linear-delayed orographic precipitation model proposed by Smith and Barstad (2004). Such a linear theory for orographic precipitation is event based, but in this case we did not directly compare this theory against our results, though valid at a climatological scale, instead we used some of the physical aspects of this theory to discuss our results.

The model of Smith and Barstad (2004) is represented by the following two steady-state condensation-advection equations:

$$\mathbf{U}\cdot\nabla q_c(\mathbf{x}) = C(\mathbf{x}) - \frac{q_c(\mathbf{x})}{\tau_c}$$

$$\mathbf{U}\cdot\nabla q_f(\mathbf{x}) = \frac{q_c(\mathbf{x})}{\tau_c} - \frac{q_f(\mathbf{x})}{\tau_f}$$

$$C(\mathbf{x}) = \rho q_v(Z)\mathbf{U}\cdot\nabla Z(\mathbf{x}), \qquad (11)$$

where $q_i(\mathbf{x})$ are the cloud (c) and hydrometeor (f) column densities (kg m^{-2}), τ_i are the characteristic time scales for cloud water conversion and hydrometeor fallout (s^{-1}), $C(\mathbf{x})$ is the source/sink condensed water term in the form proposed by Smith (1979) (kg m^{-2} s^{-1}), and $\mathbf{U}$ the regionally averaged wind vector (m s^{-1}).

Looking at Table 3 we see that in the southern French Alps and Piedmont the most important parameter, explaining most of the variance, is the elevation at the gauging station $Z(\mathbf{x})$. In fact, a large number of the gauged sites have values of L around 50 km. Assuming $|\mathbf{U}|$ and $\tau_c = \tau_f = \tau$ (Medina et al. 2005) constant across the whole homogeneous region (see section 2), whose typical values for these study regions are $|\mathbf{U}| = 10$ m s^{-1} and $\tau = 500$–1000 s (Buzzi and Foschini 2000; Barstad and Smith 2005; Smith et al. 2003) we have in this case, for most of the gauged sites, $L/|\mathbf{U}| \gg 1000\text{ s} = \tau$. As the advection terms for water densities in the left-hand side of the first two equations in (11) scale with $|\mathbf{U}|q/L$ and the conversion terms in the right-hand side scale with q/τ, for large L values such as $L/|\mathbf{U}| \gg \tau$, the advection term in Eq. (11) is small. This result is consistent with the regression results that rainfall intensity at a given location $\mathbf{x}$ depends on the local elevation, since the source term is proportional to surface atmospheric moisture.

The regression dependency for northern France both in regards to L and Z can be explained by the presence of a two-ridge terrain with a narrower ridge superposed on the windward slope of a wider and higher ridge (Fig. 9). It has been demonstrated that a narrower ridge could significantly modulate the precipitation intensity and distribution by inducing upslope ascent, leeside descent, and gravity waves (Jiang 2007). In the lee side, $C(\mathbf{x})$ becomes negative, thus reducing rainfall intensities, and Z alone cannot explain all the variability. The position along the slopes, parameterized by L, adds to the regression model the ability to discriminate between gauged sites with the same Z though located on the windward or the lee side.

For the Liguria region, however, the characteristic value of L is around 10–20 km, thus lower than 50 km. In this case $L/|\mathbf{U}| \leq 2000\text{ s} \approx \tau$. Equation (11) assigns the same order of magnitude to the advection and to the conversion terms, which means that condensed water is partially transformed into locally and partially advected rain. Rainfall intensity does not depend in this case on its position along the slope. We can reasonably assume that the total water condensed by the forced ascent, scaled with the local mountain range elevation H, and averaged along the mountain range half-width a, is a good representation of the rainfall intensity along the slope, resulting in a scale of H/a. This result is consistent with Table 3, which shows that for Liguria the most important parameter is the local slope S. Due to the small width and the smoothed representation of the mountain range, S can be considered here a good approximation of H/a.

It is also worth highlighting that the maximum value of R^2 is attained for specific directions coinciding with major storm systems, consequently this study shows how this method agrees with physically based methods that rely on the analysis and or physical modeling of climatologically relevant storms.

7. Conclusions

This paper presents a new parsimonious methodology of modeling the spatial variability of rainfall index IR_1, based on the objective extraction of the relevant orographic and meteorological features that affect

expectations of orographically induced rainfall. The key idea is to find a general objective methodology for IR_1 estimation in mountainous areas, by extracting the parameters affecting its spatial variability from a smoothed DEM, along oriented cross sections that follow the dominant low-level (700 hPa) winds during rainfall events.

The results show that by assuming linear relations between the orographic parameters used in linear models that describe orographic rainfall (widely used in literature) and neglecting the spatial variability of the climatic values of the parameters that describe atmospheric disturbances (e.g., wind speed, atmospheric moisture, etc.), it is possible to explain, through a linear regression, up to 70%–80% of the IR_1 spatial variability observed in the western Alpine region.

The results are interpreted by using a linear-convective model for orographic precipitation. This model makes it possible to identify some remarkable cases that shift the dependence of IR_1 from one orographic parameter to another. The ratio between the characteristic conversion (and fallout) time scales and the time scale of the orographic uplift seems to be the discriminant parameter, which means that the interaction between the geometry of the orographic range and the climatology of atmospheric disturbances defines the variable mainly affecting IR_1 spatial variability.

Future research activity will be devoted to the application of the proposed methodology to other portions of the Alps and Apennines. It will also be studied if this method can be enlarged, beyond relief and climatological descriptors, by adding, for example, parameters related to vegetation. Finally the performances of the method for longer duration IR_d will also be analyzed.

Acknowledgments. This research was sponsored by the National Group for prevention of natural disaster of the National Research Council (CNR-GNDCI), EU Project Interreg II France-Italy, and Regione Valle d'Aosta. The authors thank the Regione Liguria, Regione Piemonte, Regione Valle d'Aosta, and Météo-France for providing the data. The authors are grateful for the comments of the editor and the three anonymous reviewers whose help improved the manuscript.

REFERENCES

Barros, A., and D. Lettenmaier, 1993: Dynamic modeling of the spatial distribution of precipitation in remote mountainous areas. *Mon. Wea. Rev.,* **121,** 1195–1214.

——, and ——, 1994: Dynamic modeling of orographically induced precipitation. *Rev. Geophys.,* **32,** 265–284.

——, and R. Kuligowski, 1998: Orographic effects during a severe wintertime rainstorm in the Appalachian Mountains. *Mon. Wea. Rev.,* **126,** 2648–2672.

Barstad, I., and R. Smith, 2005: Evaluation of an orographic precipitation model. *J. Hydrometeor.,* **6,** 85–99.

Basist, A., and G. D. Bell, 1994: Statistical relationships between topography and precipitation patterns. *J. Climate,* **7,** 1305–1315.

Blanchet, G., 1990: Régimes météorologiques et diversité climatique dans le espace rhônalpin (Meteorological regimes and climatic variability in the area of the Alps of Rhone). *Rev. Geogr. Lyon,* **65,** 106–117.

Bobee, B., and P. F. Rasmussen, 1995: Recent advances in flood frequency analysis. *Rev. Geophys.,* **33,** 1111–1116.

Bocchiola, D., C. De Michele, and R. Rosso, 2003: Review of recent advances in index flood estimation. *Hydrol. Hearth Syst. Sci.,* **7** (3), 283–296.

Boni, G., and A. Parodi, 2002: Sintesi pluviometrica regionale: Realizzazione di un atlante sperimentale delle piogge intense sulle Alpi franco-italiane. EU Project INTERREG II Italy-France (Alps), EU Project INTERREG II Italy-France (Alps) Final Rep., 20 pp.

——, ——, and R. Rudari, 2006: Extreme rainfall events: Learning from rain gauge time series. *J. Hydrol.,* **327,** 304–314.

Bouvard, M., and H. Garros-Berthet, 1994: Les crues de projet des barrages: Methode du gradex (The flood dam project: The gradex method). Bulletin du Comite Francais des Grands Barrages, 18th ICOLD Congress, 2, 95 pp.

Buzzi, A., and L. Foschini, 2000: Mesoscale meteorological features associated with heavy precipitation in the southern Alpine region. *Meteor. Atmos. Phys.,* **72,** 131–146.

Castino, F., L. Rusca, and G. Solari, 2003: Wind climate microzoning: A pilot application to Liguria Region (North Western Italy). *J. Wind Eng. Ind. Aerodyn.,* **91,** 1353–1375.

Cavadias, G., 1990: The canonical correlation approach to regional flood estimation. *Region. Hydrol.,* **191,** 171–178.

Chow, V. T., D. R. Maidment, and L. W. Mays, 1988: *Applied Hydrology.* McGraw-Hill, 572 pp.

Collier, C. G., 1975: A representation of the effects of topography on surface rainfall within moving baroclinic disturbances. *Quart. J. Roy. Meteor. Soc.,* **101,** 407–442.

Cunnane, C., 1987: Review of statistical methods for flood frequency estimation. *Hydrologic Frequency Modeling,* V. P. Singh, Ed., D. Reidel, 49–95.

Dalrymple, T., 1960: Flood frequency analysis. U.S. Geological Survey, Water Supply Paper, 1543-A, 80 pp.

Daly, C., R. Neilson, and D. Phillips, 1994: A statistical topographic model for mapping climatological precipitation over mountainous terrain. *J. Appl. Meteor.,* **33,** 144–158.

Durbin, J., and G. S. Watson, 1950: Testing for serial correlation in least squares regression, I. *Biometrika,* **37,** 409–428.

Faulkner, D. S., and C. Prudhomme, 1998: Mapping an index of extreme rainfall across the UK. *Hydrol. Earth Syst. Sci.,* **2,** 183–194.

Ferraris, L., R. Rudari, and F. Siccardi, 2002: The uncertainty in the prediction of flash floods in the northern Mediterranean environment. *J. Hydrometeor.,* **3,** 714–727.

Ferretti, R., S. Low-Nam, and R. Rotunno, 2000: The sensitivity of numerically simulated cyclic mesocyclogenesis to variations in model physical and computational parameters. *Tellus,* **52A,** 162–180.

Fiorentino, M., S. Gabriele, F. Rossi, and P. Versace, 1987: Hierarchical approach for regional flood frequency analysis. *Regional Flood Frequency Analysis,* V. P. Singh, Ed., D. Reidel, 35–49.

Frei, C., and C. Schar, 1998: A precipitation climatology of the Alps from the high-resolution rain-gauge observations. *Int. J. Climatol.,* **18,** 873–900.

——, and ——, 2001: Detection probability of trends in rare events: Theory and application to heavy precipitation in the Alpine region. *J. Climate,* **14,** 1568–1584.

——, ——, C. Huw, J. Gurtz, and C. Schar, 2000: Climate dynamics and extreme precipitation and flood events in Central Europe. *Integr. Assess.,* **1,** 281–299.

Gabriele, S., and N. Arnell, 1991: Regional flood frequency analysis. *Water Resour. Res.,* **27** (6), 1281–1289.

Hobbs, P. V., R. Easter, and A. B. Fraser, 1973: A theoretical study of the flow of air and fallout of solid precipitation over mountainous terrain. Part II: Microphysics. *J. Atmos. Sci.,* **30,** 813–823.

Holton, J. R., 2004: *An Introduction to Dynamic Meteorology*. 4th ed. Academic Press, 535 pp.

Houze, R. A. J., C. N. James, and S. Medina, 2001: Radar observations of precipitation and airflow on the Mediterranean side of the Alps: Autumn 1998 and 1999. *Quart. J. Roy. Meteor. Soc.,* **127,** 2537–2558.

Hutchinson, M., 1998: Interpolation of rainfall data with thin plate smoothing splines—Part II: Analysis of topographic dependence. *J. Geogr. Info. Decision Anal.,* **2,** 152–167.

——, and R. J. Bischof, 1983: A new method for estimating the spatial distribution of mean seasonal and annual rainfall applied to the Hunter Valley. *Aust. Meteor. Mag.,* **31,** 179–184.

Jiang, Q., 2000: Some theoretical aspects of orographic precipitation. Ph.D. thesis, Yale University, 144 pp.

——, 2003: Moist dynamics and orographic precipitation. *Tellus,* **55A,** 301–316.

——, 2007: Precipitation over multiscale terrain. *Tellus,* **59A,** 321–335.

Johansson, B., and D. Chen, 2003: The influence of wind and topography on precipitation distribution in Sweden: Statistical analysis and modelling. *Int. J. Climatol.,* **23,** 813–823.

Journel, A. G., and C. J. Huijbregts, 1978: *Mining Geostatistics.* Academic Press, 610 pp.

Kottegoda, N. T., and R. Rosso, 1997: *Statistics, Probability and Reliability for Civil and Environmental Engineers.* McGraw-Hill, 768 pp.

Kuligowski, R., and A. Barros, 1998: Experiments in short-term precipitation forecasting using artificial neural networks. *Mon. Wea. Rev.,* **126,** 470–482.

Lin, Y.-L., S. Chiao, T. Wang, M. Kaplan, and R. Weglarz, 2001: Some common ingredients for heavy orographic rainfall. *Wea. Forecasting,* **16,** 633–660.

Marquinez, J., J. Lastraand, and P. Garcia, 2003: Estimation models for precipitation in mountainous regions: The use of GIS and multivariate analysis. *J. Hydrol.,* **270,** 1–11.

Massacand, A. C., H. Wernli, and H. C. Davies, 1998: Heavy precipitation on the Alpine southside: An upper-level precursor. *Geophys. Res. Lett.,* **25,** 1435–1438.

Medina, S., B. Smull, J. R. Houze, and M. Steiner, 2005: Cross-barrier flow during orographic precipitation events: Results from MAP and IMPROVE. *J. Atmos. Sci.,* **62,** 3580–3598.

Mertz, J., 1957: Essai de classification des types de temps sur les Alpes d'après la disposition des isohypses à 500 mb. IVème Congrès Int. de Météorologie Alpine Chamonix. *La Météorologie,* **45–46,** 305–315.

Nathan, R., and T. McMahon, 1990: Identification of homogeneous regions for the purpose of regionalisation. *J. Hydrol.,* **121,** 217–238.

Parodi, A., and G. Boni, 2001: Phenomenological validation of a regional rainfall frequency analysis. *Phys. Chem. Earth,* **26B,** 649–654.

Reed, D., 1994: Plans for the flood estimation handbook. *Proc. MAFF Conf. of River and Coastal Engineers,* Loughborough, London, MAFF, 8.3.1–8.3.8.

Renard, B., and M. Langa, 2007: Use of a Gaussian copula for multivariate extreme value analysis: Some case studies in hydrology. *Adv. Water Resour.,* **30,** 897–912.

Roe, G. H., 2005: Orographic precipitation. *Annu. Rev. Earth Planet. Sci.,* **33,** 645–671.

Rosso, R., and P. Burlando, 1996: Scaling and multiscaling models of depth-duration-frequency curves for storm precipitation. *J. Hydrol.,* **187,** 45–64.

Rotunno, R., and R. Ferretti, 2001: Mechanisms of intense Alpine rainfall. *J. Atmos. Sci.,* **58,** 1732–1749.

Rudari, R., D. Entekhabi, and G. Roth, 2004: Terrain and multiple-scale interactions as factors in generating extreme precipitation events. *J. Hydrometeor.,* **5,** 390–404.

——, ——, and ——, 2005: Large-scale atmospheric patterns associated with mesoscale features leading to extreme precipitation events in Northwestern Italy. *Adv. Water Resour.,* **28** (6), 601–614.

Sawyer, J. S., 1956: The physical and dynamical problems of orographic rain. *Weather,* **11,** 375–381.

Schiesser, H., R. Houza, and H. Huntrieser, 1995: The mesoscale structure of severe precipitation systems in Switzerland. *Mon. Wea. Rev.,* **123,** 2070–2097.

Sharples, J., M. Hutchinson, and R. J. Damian, 2005: On the horizontal scale of elevation dependence of Australian monthly precipitation. *J. Appl. Meteor.,* **44,** 1850–1865.

Siccardi, F., G. Boni, L. Ferraris, and R. Rudari, 2005: A hydrometeorological approach for probabilistic flood forecast. *J. Geophys. Res.,* **110,** D05101, doi:10.1029/2004JD005314.

Smith, R., 1979: The influence of mountains on the atmosphere. *Advances in Geophysics,* Vol. 21, Academic Press, 87–229.

——, and I. Barstad, 2004: A linear theory of orographic precipitation. *J. Atmos. Sci.,* **61,** 1377–1391.

——, Q. Jiang, M. G. Fearon, P. Tabary, M. Dorninger, J. Doyle, and R. Benoit, 2003: Orographic precipitation and air mass transformation: An Alpine example. *Quart. J. Roy. Meteor. Soc.,* **129,** 433–454.

Spreen, W., 1947: The influence of mountains on the atmosphere. *Eos, Trans. Amer. Geophys. Union,* **28,** 285–290.

Stewart, E. J., D. W. Reed, D. S. Faulkner, and N. S. Reynard, 1999: The FORGEX method of rainfall growth estimation I: Review of requirement. *Hydrol. Earth Syst. Sci.,* **3,** 187–195.

Tabios, G. Q., and J. D. Salas, 1985: A comparative analysis of techniques for spatial interpolation of precipitation. *Water Resour. Bull.,* **21,** 365–380.

Tibaldi, S., and A. Buzzi, 1983: Effects of orography on Mediterranean lee cyclogenesis and its relationship to European blocking. *Tellus,* **35A,** 269–286.

——, and F. Molteni, 1990: On the operational predictability of blocking. *Tellus,* **42A,** 343–365.

Weisse, A., and P. Bois, 2001: Topographic effects on statistical characteristics of heavy rainfall and mapping in the French Alps. *J. Appl. Meteor.,* **40,** 720–740.

Wotling, G., C. Bouvier, J. Danloux, and J.-M. Fritsch, 2001: Regionalization of extreme precipitation distribution using the principal components of the topographical environment. *J. Hydrol.,* **233,** 86–101.